

# Concepts from Representations: Post-hoc Concept Bottleneck Models via Sparse Decomposition of Visual Representations

Shizhan Gong<sup>1</sup>, Xiaofan Zhang<sup>2</sup>, Qi Dou<sup>1</sup>

<sup>1</sup>The Chinese University of Hong Kong, Hong Kong, China

<sup>2</sup>Shanghai Jiao Tong University, Shanghai, China

szgong22@cse.cuhk.edu.hk, xiaofan.zhang@sjtu.edu.cn, qidou@cuhk.edu.hk

## Abstract

Deep learning has achieved remarkable success in image recognition, yet their inherent opacity poses challenges for deployment in critical domains. Concept-based interpretations aim to address this by explaining model reasoning through human-understandable concepts. However, existing post-hoc methods and ante-hoc concept bottleneck models (CBMs), suffer from limitations such as unreliable concept relevance, non-visual or labor-intensive concept definitions, and model/data-agnostic assumptions. This paper introduces **Post-hoc Concept Bottleneck Model via Representation Decomposition (PCBM-ReD)**, a novel pipeline that retrofits interpretability onto pretrained opaque models. PCBM-ReD automatically extracts visual concepts from a pre-trained encoder, employs multimodal large language models (MLLMs) to label and filter concepts based on visual identifiability and task relevance, and selects an independent subset via reconstruction-guided optimization. Leveraging CLIP’s visual-text alignment, it decomposes image representations into linear combination of concept embeddings to fit into the CBMs abstraction. Extensive experiments across 11 image classification tasks show PCBM-ReD achieves state-of-the-art accuracy, narrows the performance gap with end-to-end models, and exhibits better interpretability.

Code — [https://github.com/peterant330/PCBM\\_ReD](https://github.com/peterant330/PCBM_ReD)

## 1 Introduction

Deep learning has made significant strides in various image recognition tasks. However, the complexity of these models, which is often necessary to achieve high accuracy, leads to an opaque behavior. This limits the broader application in critical fields such as medical imaging analysis (Gong et al. 2025b) and autonomous driving (Omeiza et al. 2021). Concept-based interpretation is a subfield of explainable artificial intelligence that aims to use human understandable concepts to explain the model behaviors. Concept-based methods usually represent the semantic features learned by the network with concept labels, so that human can understand which features are responsible for the final predictions.

Concept-based methods can be divided into post-hoc methods and ante-hoc approaches (Fig. 1). Post-hoc meth-

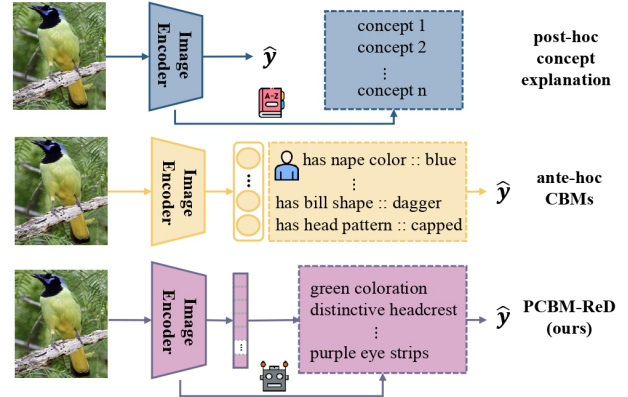


Figure 1: PCBM-ReD extracts concepts from the pre-trained image encoder and reconstruct the visual representation with the concepts, which gives faithful interpretation and can take the best advantage of the encoder’s representation power.

ods associate latent space representations to human-understandable concepts, either supervised with user-defined concepts (Bau et al. 2017; Fong and Vedaldi 2018) or by unsupervised pattern recognition (Ge et al. 2021; Vielhaben, Bluecher, and Strodthoff 2023). However, these methods face some major limitations. Firstly, there is no guarantee that the extracted concepts faithfully reflect the reasoning process of the network. Additionally, there may be no intuitive and human-understandable causal relationship between the extracted concepts and targets, making it difficult for users to understand the mechanism of the network. Moreover, automated concepts mining process can generate a great number of concepts with low semantic value, which are difficult to be labeled by humans (Kim et al. 2018).

Concept Bottleneck Models (CBMs) (Koh et al. 2020) are ante-hoc approaches that integrate concept associations into neural networks through modifications in model design or training. They predict a set of interpretable concepts and use a linear function to generate final predictions based on these concepts. This structure allows users to trace the links between concepts and class labels, facilitating error correction. CBMs rely on user-defined concepts, which can be either manually crafted by experts (Koh et al. 2020; Yun et al.

2022) or generated by large language models (LLMs) (Yang et al. 2023; Oikarinen et al. 2023). However, the current CBMs exhibit several weaknesses: human-crafted concepts can be labor-intensive and may lack comprehensive coverage (Koh et al. 2020), while LLMs-generated concepts often include non-visual features (e.g., the taste of food or bird behavior, which are not visually inferred) (Yang et al. 2023). Additionally, these pre-defined concepts are data-independent and model-agnostic, which can hinder their effectiveness, especially if a dataset is biased towards certain subpopulation or if the image encoder cannot capture certain features (e.g., color or spatial relationships (Kamath, Hessel, and Chang 2023)). Furthermore, current methods do not guarantee the independence of generated concepts, which is essential for effective interventions in CBMs. These limitations hinder CBMs from achieving complete feature space interpretability (Kim et al. 2018).

In this work, we introduce a novel pipeline that retrofits interpretability onto pretrained opaque foundation models, called **Post-hoc Concept Bottleneck Model via Representation Decomposition (PCBM-ReD)**. Given a pre-trained image encoder, we first apply automatic concept extraction (Fel et al. 2023) to mine the generalizable features encoded within the foundation models. To further ensure they are visually-identifiable, human-understandable, and task-related, we use multimodal large language models (MLLMs) to label concepts by summarizing descriptions of top-activated images for each concept and scoring them based on prior knowledge of the task. We then propose a reconstruction-guided concept selection algorithm that selects a subset of concepts, whose embedding spans are independent and completely define the visual representation space. For image-concept association, we utilize the visual-text alignment property of CLIP (Radford et al. 2021), which allows us to decompose the visual representation into a weighted sum of the concepts’ text embeddings. By eliminating residual terms and fitting a linear function to the reconstructed representation, we can develop a model that adheres to the abstractions of CBMs while preserving the representational power of the original opaque visual encoder.

We conduct comprehensive experiments to demonstrate the efficacy of our proposed method. We evaluate the model performance on 11 image classification tasks, including common object recognition, fine-grained types, texture, and action classification, as well as domain-specific tasks such as medical diagnosis and satellite image object recognition. Our main finding is that the model achieves state-of-the-art classification accuracy, with a reduced gap compared to end-to-end models, compared to existing CBMs. Furthermore, as we aim to mimic the behavior of the end-to-end model using CBM, our approach exhibits similar properties, including zero-shot and few-shot capabilities. Additionally, we conduct human evaluation to demonstrate the improved interpretability of PCBM-ReD. Our main contributions include:

- We propose a data-driven scheme for creating and selecting concepts that align with the data distribution and the image encoder’s representation capabilities.
- We propose constructing CBMs by leveraging CLIP’s

visual-text alignment to sparsely decompose the visual representation into concept embeddings.

- We demonstrate that PCBM-ReD achieves SOTA classification accuracy across various tasks, along with better interpretability and robust zero/few-shot capabilities.

## 2 Related Work

**Explanations in Computer Vision.** Explainable computer vision primarily falls into two categories: post-hoc explanations and interpretable models by design. Post-hoc explanation methods generate saliency maps to identify which input features influence the decisions of neural networks (Simonyan, Vedaldi, and Zisserman 2013; Selvaraju et al. 2017; Gong, Dou, and Farnia 2024; Gong et al. 2025a). However, these methods do not guarantee that the explanations faithfully reflect the model’s reasoning process (Rudin 2019). In contrast, interpretable models by design ensure that explanations align with the models’ reasoning (Chen et al. 2019; Nauta, Van Bree, and Seifert 2021; Ma et al. 2024; Tan, Zhou, and Chen 2024b). Our work builds upon CBMs (Koh et al. 2020), a type of interpretable models.

**Concept Bottleneck Models.** CBMs (Koh et al. 2020; Zarlenga et al. 2022; Kim et al. 2023; Gong et al. 2025b) predict outcomes by linearly combining an intermediate layer of human-understandable attributes. The original CBM relies on handcrafted and manually annotated attributes. CompDL (Yun et al. 2022) replaces manual annotations with CLIP scores, but still depends on concepts designed by human. LaBo (Yang et al. 2023) and label-free CBM (Oikarinen et al. 2023) further automate concept generation using LLMs. Early CBMs often underperformed compared to end-to-end models. To improve it, Post-hoc CBM (Yuksekgonul, Wang, and Zou 2022) introduces a residual connection from image features to predictions, while Res-CBM (Shang et al. 2024) approximates this connection by incrementally adding new concepts. OpenCBM (Tan, Zhou, and Chen 2024a) detects missing concepts from an open vocabulary. Our method reduces residuals from the beginning by mining concepts that can well reconstruct the image representations.

**CLIP Interpretation.** CLIP (Radford et al. 2021) utilizes contrastive learning on a large dataset of paired text and images to link images with their textual descriptions. This approach effectively groups similar concepts together and shows strong performance in downstream tasks, such as zero-shot classifications (Saha, Van Horn, and Maji 2024). Several studies focusing on the interpretation of CLIP have shown that its homogeneous feature space allows the visual embeddings to be decomposed into multiple concepts represented by concepts’ text embeddings (Moayeri et al. 2023; Chen et al. 2023; Gandelsman, Efros, and Steinhardt 2023, 2024). This provides the theoretical foundation for our method, which constructs CBMs by directly decomposing visual representations into concepts representation, thus better preserving predictive power.

## 3 Method

Consider a training set of image-label pairs  $\mathcal{D} = \{(\mathbf{x}, y) \in \mathbb{R}^{d_x} \times \mathcal{Y}\}$ , and a bottleneck  $C$  made of  $N_C$  concepts,

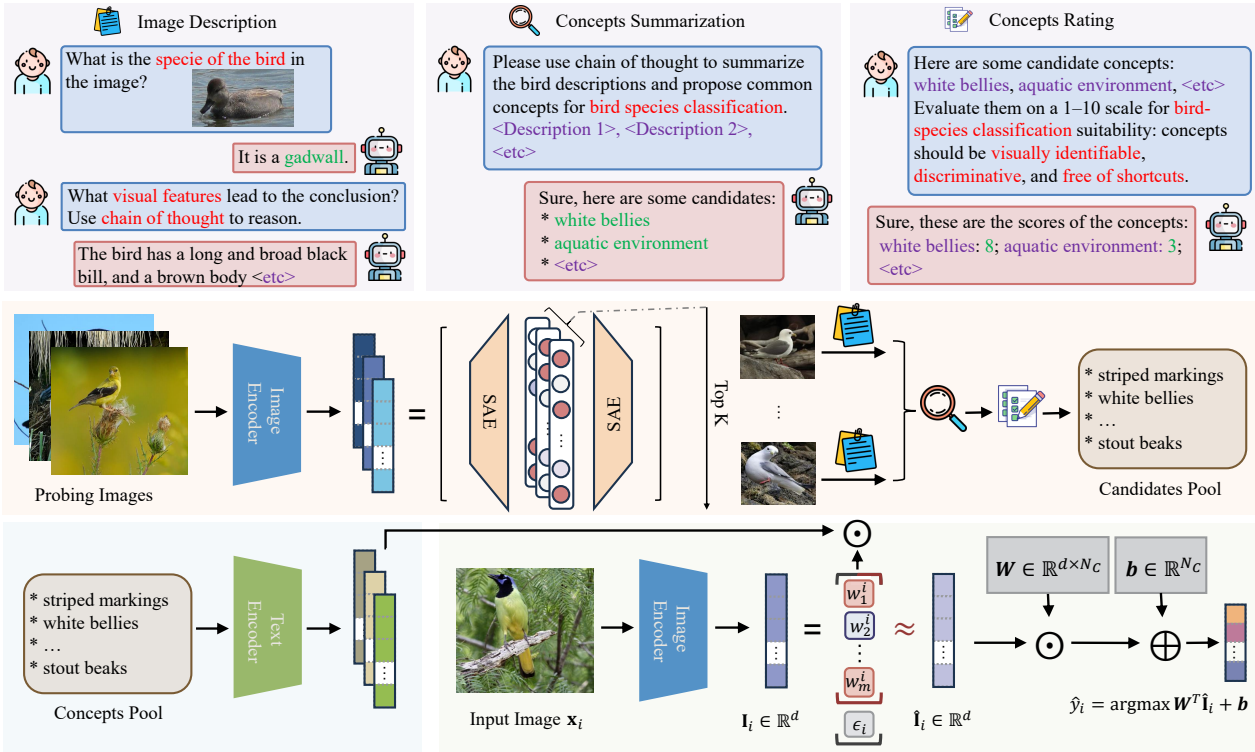


Figure 2: We present an overview of **Post-hoc Concept Bottleneck Model** via **Representation Decomposition (PCBM-ReD)**. First, we extract concepts from the learned representation, and use MLLMs to summarize and score the concepts. Second, we apply a concept selection algorithm to choose concepts and construct the bottleneck. Third, we perform sparse decomposition and reconstruct the image embedding by concepts. A linear layer is trained to predict the targets with the fitted embedding.

$C := \{c_1, c_2, \dots, c_{N_C}\}$ . CBM make prediction by composing two functions,  $\hat{y} = f(g(\mathbf{x}))$ , where  $g : \mathbb{R}^{d_x} \rightarrow \mathbb{R}^{N_C}$  maps  $\mathbf{x}$  to a score for each element of the bottleneck, and  $f : \mathbb{R}^{N_C} \rightarrow \mathcal{Y}$  makes the final prediction on the label space given the concept scores. Fig. 2 presents an overview.

### 3.1 Data-driven Concept Discovery

Most existing methods for constructing bottlenecks rely on either handcrafted concepts (Koh et al. 2020) or concepts generated by LLMs (Yang et al. 2023). However, these concept creation processes are typically independent of the training data or the image encoder, which can result in sub-optimal concepts that fail to capture variations in specific data distributions or are challenging for the visual encoder to distinguish. To overcome these limitations, we propose an approach that automatically extracts concepts from a pre-trained image encoder. We leverage the pre-trained multi-modal alignment model, CLIP (Radford et al. 2021), which consists of an image encoder  $\mathcal{I}$  and a text encoder  $\mathcal{T}$ . The image encoder transforms an image  $\mathbf{x}_i$  into a representation  $\mathbf{I}_i = \mathcal{I}(\mathbf{x}_i) \in \mathbb{R}^d$ . If the encoder effectively captures structured patterns, its latent space should be disentangled into subspaces representing distinct concepts (Bau et al. 2017; Oikarinen and Weng 2022). To do so, we apply sparse autoencoder (SAE) (Bricken et al. 2023), which enables us to represent the visual embedding  $\mathbf{I}_i$  with the concept bank

atoms  $\mathbf{u}_i \in \mathbb{R}^k$ , such that  $\mathbf{I}_i \approx \mathbf{V}\mathbf{u}_i$ . The SAE represents  $\mathbf{u}_i$  by a neural network  $\psi$  (i.e.,  $\mathbf{u}_i = \psi(\mathbf{I}_i)$ ) and enforces sparsity on  $\mathbf{u}_i$  (Fel et al. 2023), known to effectively address the challenge of polysemy (Bricken et al. 2023). Other dictionary learning paradigms are also applicable.

Ideally, each column of  $\mathbf{V}$  represents a concept and the corresponding value of  $\mathbf{u}_i$  reflects the significance of the concept in  $\mathbf{I}_i$ . To transform the concepts into human-understandable form, we propose a MLLM-based pipeline for labeling and scoring the concepts. We sample a reasonable number of images from the training data as probing images, and obtain their corresponding  $\mathbf{u}_i$ . Then for each concept, we select the top  $K$  images with largest concept scores. We then prompt the MLLMs with chain-of-thought to summarize the concept. As shown in Fig. 2, for each image, we prompt MLLMs to describe the visual features that can help identify the category of the image. After collecting image descriptions for the top  $K$  images, we ask LLMs to summarize these descriptions and generate candidate concepts that is useful for a specific classification problem. This process results in a large number of candidate concepts, which may or may not be good concepts for the classification tasks. We then ask LLMs to score these concepts. We prompt the LLMs to only assign high scores to concepts that are visually identifiable, discriminatory, and free of shortcuts (e.g., concepts describing the background). We filtered out candi-

Method	Interpret.	ImageNet	CIFAR10	CIFAR100	FOOD	Aircraft	Flower	CUB	UCF	DTD	HAM	RESISC	Average
<b>Fully-supervised Setting</b>													
Linear Probe	✗	83.90	98.10	87.48	93.17	64.03	99.45	84.54	90.67	81.68	83.18	94.98	87.38
LaBo	✓	83.97	97.75	86.04	92.45	61.42	99.35	81.90	90.11	77.30	<b>81.39</b>	91.22	85.72
Res-CBM	✓	82.98	97.77	83.01	90.17	54.67	97.85	79.27	88.37	75.77	75.72	91.67	83.39
V2C-CBM	✓	84.15	98.03	86.41	92.84	60.71	98.94	83.12	-	78.49	81.12	92.86	-
PCBM-ReD (ours)	✓	<b>84.48</b>	<b>98.05</b>	<b>87.27</b>	<b>93.16</b>	<b>62.95</b>	<b>99.39</b>	<b>84.80</b>	<b>90.38</b>	<b>81.44</b>	<b>81.39</b>	<b>93.31</b>	<b>86.97</b>
<b>Zero-shot Classification Setting</b>													
CLIP	✗	72.90	95.57	78.28	90.91	31.77	79.46	62.19	75.31	57.09	58.21	64.87	69.69
PCBM-ReD (ours)	✓	72.89	95.56	78.24	90.91	32.01	79.58	62.03	75.36	57.09	58.51	64.87	69.73
CuPL	✗	73.45	95.82	78.59	91.23	35.43	80.80	64.43	76.00	62.65	57.91	71.88	71.65
PCBM-ReD + CuPL (ours)	✓	73.43	95.80	78.59	91.22	35.52	80.67	64.62	75.91	62.77	58.11	71.88	71.68

Table 1: Test accuracy (%) of PCBM-ReD on 11 image classification benchmarks. We report performance of both fully-supervised setting and zero-shot setting. For fully-supervised setting, we compare PCBM-ReD with linear probe, LaBo and Res-CBM. For zero-shot setting, we utilize two strategies, i.e., vanilla CLIP and CuPL. CLIP ViT-L/14 is used as the backbone.

dates with low scores, leaving only high-quality concepts.

### 3.2 Reconstruction-guided Concept Selection

The LLM-based scoring ensures that the resulting concepts are both human-understandable and relevant to specific tasks. However, the use of a limited sample size for summarizing these concepts can result in noisy outputs with low coverage of the overall dataset. Moreover, the candidate pool may include overlapping or repetitive concepts. To address these issues, it is crucial to select a subset of important and independent concepts that can still comprehensively cover the entire representation space.

We take a set of  $N$  probing images sampled from the training data, with  $\mathbf{I}_1, \dots, \mathbf{I}_N$  denoting their image embeddings in the joint text-image space. Given a collection of concepts  $\mathcal{C}$ , we can reconstruct the image representations by linear combination of the text representations of the concepts within the concept set (denoted as  $\mathbf{R}(\mathcal{C}) \in \mathbb{R}^{M_C \times d}$ ). We further define the reconstruction error to be the Frobenius norm of the difference between the original and the reconstructed image embedding. Our goal is to identify the optimal subset that minimize the reconstruction error:

$$\min_{\mathcal{C}} \sum_{i=1}^N \min_{\beta_i(\mathcal{C})} \|\mathbf{I}_i - \mathbf{R}(\mathcal{C})^T \beta_i(\mathcal{C})\|_F^2, \quad (1)$$

where  $\beta_i(\mathcal{C})$  is the coefficients of linear combination for reconstructing  $\mathbf{I}_i$ . While the subset selection is a discrete optimization problem without close-form solution, we propose a greedy algorithm that select concepts step-wisely. Additionally, although the inner optimization of coefficients  $\beta_i$  has analytical solution, we need to solve the optimization problem for each concept within the set  $\mathcal{C}$ , which can be computational-intensive when the size of  $\mathcal{C}$  is large. We propose an algorithm for efficient computation, as illustrated in

Alg. 1. Detailed explanation of the algorithm can be found in Appendix. The algorithm can incrementally select new concepts, minimizing reconstruction error to the greatest extent, while ensuring that the newly added concepts are linearly independent from the existing ones. The algorithm stops when the selected concepts reach a pre-defined value, or when all new concepts are linearly dependent on the existing concepts. It is important to note that, unlike the selection algorithms presented in previous work (Chen et al. 2019; Yang et al. 2023), this selection scheme is entirely unsupervised, making it suitable for zero/few-shot applications.

### 3.3 Post-hoc Class-concept Association

**Concept Scores Assignment.** Multimodal learning enables the alignment of representations from different modalities into a joint space. Several studies (Gandelsman, Efros, and Steinhardt 2023, 2024) have demonstrated that the image embeddings of CLIP can be represented as a weighted sum of text representations. Therefore, rather than relying on manual annotations or text-image similarity scores to generate concept score supervision, we propose to directly decompose the image representation into concept-related directions within the joint representation space. To ensure high interpretability, we aim for this decomposition to be sparse, utilizing only a few key concepts to explain the image representation. Mathematically, we express this as:

$$\mathbf{I}_i = \hat{\mathbf{I}}_i + \epsilon_i = \sum_{j=1}^m w_j^i \mathbf{c}_j + \epsilon_i, \quad (2)$$

where  $\mathbf{c}_j$  is the embedding of concept  $c_j$  and  $\epsilon_i$  is residue. We apply a sparse coding algorithm (e.g., orthogonal matching pursuit (Pati, Rezaifar, and Krishnaprasad 1993)) to approximate  $\mathbf{I}_i$  as the sum above, where only  $n$  of the  $w_j^i$  are non-zero, for some  $n < m$ .

---

**Algorithm 1: Concepts Selection Algorithm**


---

**Input:** Image embedding for  $N$  images stacked as rows in a matrix  $\mathbf{X} \in \mathbb{R}^{N \times d}$ , a pool of  $M$  concepts  $\{c_i\}_{i=1}^M$ , their corresponding text representations  $\{\mathcal{T}(c_i)\}_{i=1}^M$ , selected concepts size  $m$ , identity matrix  $\mathbf{E}$

**Output:** A set of selected candidates  $\mathcal{C}$

**Initialization:**  $\mathcal{C} \leftarrow \emptyset, \mathcal{C}_0 \leftarrow \{c_i\}_{i=1}^M$

$$c^* \leftarrow \arg \max_{c \in \mathcal{C}_0} \left\| \mathbf{X} \cdot \left( \mathbf{E} - \frac{\mathcal{T}(c)\mathcal{T}(c)^T}{\mathcal{T}(c)^T \mathcal{T}(c)} \right) \right\|_F^2$$

$$\mathcal{C} \leftarrow \mathcal{C} \cup \{c^*\}, \mathcal{C}_0 \leftarrow \mathcal{C}_0 \setminus \{c^*\}$$

**for**  $i$  in  $[2, \dots, m]$  **do**

$$\mathbf{P} \leftarrow \mathbf{R}(\mathcal{C})(\mathbf{R}(\mathcal{C})^T \mathbf{R}(\mathcal{C}))^{-1} \mathbf{R}(\mathcal{C})^T$$

**for**  $c$  in  $\mathcal{C}_0$  **do**

$$\quad z \leftarrow \mathcal{T}(c)^T (\mathbf{E} - \mathbf{P}) \mathcal{T}(c)$$

**if**  $z = 0$  **then**

$$\quad \quad \mathcal{C}_0 \leftarrow \mathcal{C}_0 - \{c\}$$

**else**

$$\quad \quad \mathbf{Q} \leftarrow \mathcal{T}(c)\mathcal{T}(c)^T / z$$

$$\quad \quad \mathbf{L}(c) \leftarrow \mathbf{P}\mathbf{Q}\mathbf{P} - \mathbf{Q}\mathbf{P} - \mathbf{P}\mathbf{Q} + \mathbf{P} + \mathbf{Q}$$

**if**  $\mathcal{C}_0 = \emptyset$  **then**

**break**

$$c^* \leftarrow \arg \min_{c \in \mathcal{C}_0} \left\| \mathbf{X} (\mathbf{E} - \mathbf{L}(c)) \right\|_F^2$$

$$\mathcal{C} \leftarrow \mathcal{C} \cup \{c^*\}, \mathcal{C}_0 \leftarrow \mathcal{C}_0 \setminus \{c^*\}$$


---

**Label Predictor.** After decompose each image embedding  $\mathbf{I}_i$  into the sum of concept embedding, we discard the residue and retain only the fitted representation  $\hat{\mathbf{I}}_i$ . We then fit a linear layer to predict the class label from the fitted representation, expressed as  $\hat{y}_i = \arg \max (\mathbf{W}^T \hat{\mathbf{I}}_i + \mathbf{b})$ . This function can be reformulated as  $\hat{y}_i = \arg \max (\sum_{j=1}^m w_j^i \mathbf{W}^T \mathbf{c}_j + \mathbf{b})$ . As a result, it satisfies the CBM abstraction, with the coefficients  $[w_1^i, \dots, w_m^i]$  representing the concept scores, and  $\mathbf{W}^T [\mathbf{c}_1, \dots, \mathbf{c}_m]$  serving as the class-concept weight matrix. Unlike traditional CBMs that train a sparse class-concept weight matrix to improve the model interpretability, our method enforces sparsity on the concept score side by applying sparse decomposition to the visual representation.

**Weight Matrix Initialization.** Since  $\hat{\mathbf{I}}_i$  is an approximation of  $\mathbf{I}_i$ , it shares similar properties with  $\mathbf{I}_i$ . One advantage of  $\mathbf{I}_i$  is its zero-shot capability, stemming from the alignment of image and text representations. Ideally,  $\hat{\mathbf{I}}_i$  would exhibit similar zero-shot ability. To better leverage this zero-shot prior, we propose to initialize  $\mathbf{W}$  with the text embeddings of the prompt “This is a photo of [cls]”.

## 4 Experiments

### 4.1 Dataset and Baselines

Following the benchmark proposed by (Yang et al. 2023), we use 11 image classification datasets spanning a diverse set of domains, including (1) Common objects: ImageNet (Deng et al. 2009), CIFAR-10 and CIFAR-100 (Krizhevsky, Hinton et al. 2009); (2) Fine-grained objects: Food-101 (Bossard, Guillaumin, and Van Gool 2014), FGVC-Aircraft (Maji et al. 2013), Flower-102 (Nilsback and Zisserman 2008), CUB-200-2011 (Wah et al. 2011); (3) Actions: UCF-101 (Soomro 2012); (4) Textures: DTD (Cimpoi et al. 2014); (5) Skin tumors: HAM10000 (Tschandl,

Method	Interpret.	CIFAR10	CIFAR100	CUB	Average
		88.80	70.10	72.14	77.01
Linear Probe	✗				
Original CBM	✓	-	-	65.13	-
CompDL	✓	-	-	54.19	-
PCBM	✓	84.50	56.00	63.63	68.04
Label-free CBM	✓	86.40	65.13	62.40	71.31
CDM	✓	86.50	67.60	<b>72.26</b>	75.45
DN-CBM	✓	87.60	67.50	68.38	74.49
VLG-CBM	✓	<b>88.63</b>	66.48	66.03	73.71
PCBM-ReD (ours)	✓	88.61	<b>70.03</b>	72.01	<b>76.88</b>

Table 2: Test accuracy (%) comparison between PCBM-ReD and baselines for fully-supervised setting. We use CLIP RN50 as the backbone for all methods.

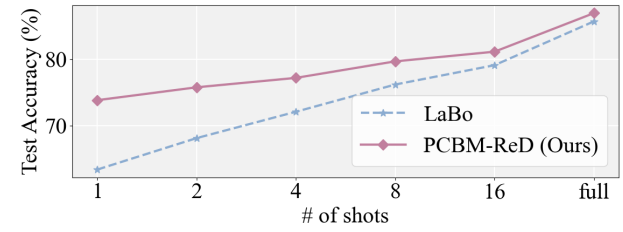


Figure 3: Few-shot test accuracy (%) comparison. Average test accuracy on 11 datasets is reported. Shot means the number of labeled images for each class.

Rosendahl, and Kittler 2018), and (6) Satellite images: RESISC45 (Cheng, Han, and Lu 2017). We use the same train/dev/test splits as (Yang et al. 2023) for all datasets. For all experiments, we train on the training set and report the test accuracy. We compare our model, PCBM-ReD, with end-to-end linear probing, as implemented from CLIP (Radford et al. 2021), as well as several CBMs, including original CBM (Koh et al. 2020), PCBM (Yuksekgonul, Wang, and Zou 2022), CompDL (Yun et al. 2022), label-free CBM (Oikarinen et al. 2023), LaBo (Yang et al. 2023), Res-CBM (Shang et al. 2024), CDM (Panousis, Ienco, and Marcos 2023), DN-CBM (Rao et al. 2024), V2C-CBM (He et al. 2025), and VLG-CBM (Srivastava, Yan, and Weng 2024).

### 4.2 Implementation Details

We use Llama-3.2-11B-Vision-Instruct to generate image descriptions and use DeepSeek-V3 to summarize and score the concepts. We use CLIP models from OpenCLIP (Cherti et al. 2023) with ViT-L/14 as the default backbone. To train the linear head, we use Adam optimizer with the batch size of 64 and the learning rate of  $5 \times 10^{-5}$ . All experiments were conducted on NVIDIA GeForce RTX 4090 GPUs. More details are provided in the Appendix.

	Class Name	Top Concepts	Class Name	Top Concepts	Class Name	Top Concepts	Class Name	Top Concepts
ImageNet	cock	1. an animal with a black-tipped tail 2. a bird with intricate plumage and orange beak 3. bird with ruffled feathers	Tibetan terrier	1. a dark brown creature with black and white stripes 2. an animal with a black-tipped tail 3. a black dog with a short snout	basson	1. a long-handled tool 2. a cylindrical tube with a shiny finish 3. a polished gold or silver musical instrument	notebook	1. rectangular device with round corners and screen 2. a QWERTY keyboard layout 3. black and white device with buttons
CUB	horned puffin	1. distinctive beak shapes and curves 2. black and white plumage 3. yellow beak with colored tip	frigatebird	1. glossy black bird with long beaks 2. white bellied bird with black markings 3. black and vivid color combinations	nighthawk	1. brown and gray color patterns 2. distinctive white stripes above eyes 3. prominent eye patterns	forsters tern	1. long, distinctive tails 2. blue-gray plumage with white belly 3. orange legs and feet
Flower	passion flower	1. flower with a central stamen 2. purple-colored flowers 3. unique corona structures of Passiflora genus	purple coneflower	1. thistle-like blooms 2. red and yellow flowers 3. long, pointed purple petals	peruvian lily	1. dark purple centres with yellow stamens 2. thin, long stamens 3. flowers with a pouch-like structure	gazania	1. vibrant petals in a spiral pattern 2. large, bright yellow flowers with dark centers 3. yellow petals with red veining
HAM10000	basal cell carcinoma	1. mix of brown, black, gray colors 2. brown area surrounded by pinkish hue 3. darker brown dots and globules	melanocytic nevi	1. mix of brown, black, gray colors 2. central darker area and lighter periphery 3. notched and irregular shape	melanoma	1. brownish-red patch and white surrounding area 2. darker brown center 3. multicomponent pigmented lesion	vascular lesions	1. brown dots and globules 2. combination of brown and pink colors 3. a lighter periphery

Figure 4: Several example explanations generated by PCB-M-ReD. The examples are sampled from the test set of 11 datasets, which have correct predictions. We also show their corresponding top concepts that contribute the most to the logits.

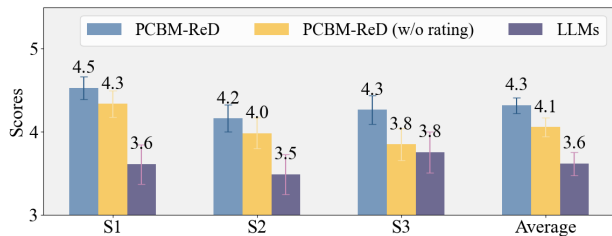


Figure 5: Human evaluation. Volunteers rate the explanation on a scale of 1 to 5 (5 = very agree). **S1:** The explanations are visually identifiable features. **S2:** The explanations faithfully describe the image. **S3:** There is a causal relationship between the explanation and the prediction.

### 4.3 Main Results

**Comparison with End-to-end Model.** Table 1 presents the test accuracy of both PCB-M-ReD and the linear probe. Our findings indicate that the performance difference between PCB-M-ReD and the linear probe is minimal, with an average test accuracy that is just 0.41% lower, despite improved interpretability. Notably, for several datasets, PCB-M-ReD even outperforms the end-to-end model. In general, the performance of PCB-M-ReD is affected by the concepts, which in turn depend on the quality of the description. For datasets like HAM, general MLLMs may struggle to accurately describe the skin tumors using specific terminology. Domain-specific MLLMs may further improve the performance.

**Comparison with other CBMs.** We also compare PCB-M-ReD’s performance with other CBMs in Table 1 and 2. PCB-M-ReD outperforms other language-guided CBMs such as LaBo and label-free CBM. It shows an average test accuracy that is 1.25% higher than LaBo and 5.57% higher than label-free CBM. It also achieves greater accuracy than CompDL and the original CBM, even though it does not depend on manually constructed concepts and annotations.

### 4.4 Performance on Low-data Regime

**Zero-shot Ability.** Since the weighted sum of concept embeddings approximates the original image embeddings, it retains zero-shot capabilities similar to the original embeddings, something existing CBMs typically lack. In Table 1, we present zero-shot accuracy using two strategies: the vanilla approach from CLIP and CuPL (Pratt et al. 2023). For comparison, we include the performance of the original CLIP representation. The results show that our method achieves strong zero-shot performance, with average accuracy comparable to CLIP, while being interpretable.

**Few-shot Performance.** We also evaluate the few-shot performance of PCB-M-ReD across various datasets. We follow the few-shot evaluation protocol proposed by CLIP with 1, 2, 4, 8, and 16 images randomly sampled from the training set for each class. In Fig. 3, we present the average test accuracy, alongside the accuracy of LaBo for comparison. The full results can be found in Appendix. The results show PCB-M-ReD consistently outperform LaBo. On average, PCB-M-ReD surpasses LaBo by 5.01%. This shows the potential application of our methods in few-shot learning.

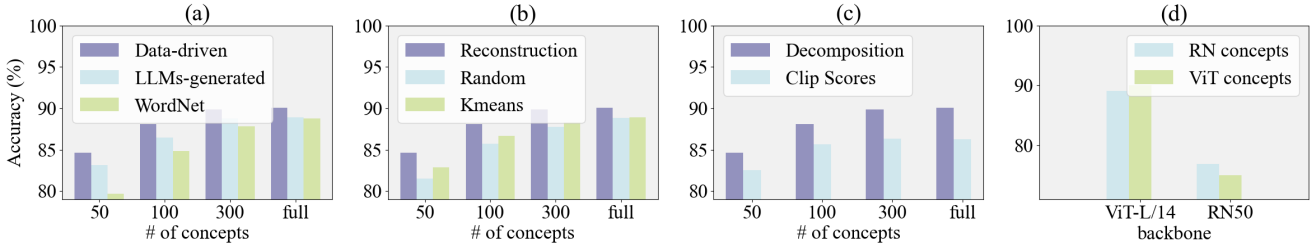


Figure 6: Ablation studies. (a) Test accuracy with different creation schemes of the concepts and the size of the bottleneck. (b) Comparison between reconstruction-guided concept selection, random sampling, and K-Means. (c) Comparison between decomposition-based and CLIP similarity-based concept score association. (d) Effects of sources of the extracted concepts.

#### 4.5 Interpretation Evaluation

**Qualitative Analysis.** To evaluate PCB-M-ReD’s interpretability, we present examples illustrating its reasoning process. In Fig. 4, we visualize test set images alongside the top three concepts that most significantly contribute to the correct class’s logit. The results show that PCB-M-ReD effectively identifies key concepts in the images, which reliably predict corresponding labels. Furthermore, the concepts adapt to different data distributions. For general tasks like ImageNet classification, broad concepts (e.g., color, class) suffice to differentiate categories. In contrast, fine-grained classification requires more specific details (e.g., object parts). Additionally, the concepts are derived directly from visual features, which further enhances the interpretability.

**Human Evaluation.** We conduct a user study to evaluate the quality of the extracted concepts and generated explanations. Images from five datasets (Imagenet, Food-101, UCF-101, CUB-200-2011, and Flower-102) are randomly selected, and users are shown the image, prediction, and top concepts as explanations. Users rate the explanations on a scale of 1 to 5 based on: 1) whether the concepts are visually identifiable, 2) whether the concepts faithfully describe the image, and 3) whether the explanations have a clear causal link to class labels. Details of the study design are in the Appendix. For comparison, we evaluate explanations using concepts generated by prompting LLMs to describe the class based solely on prior knowledge without training image access (Yang et al. 2023), and PCB-M-ReD without LLM-based concept rating. Results from 39 volunteers (Fig. 5) show that PCB-M-ReD, which extracts concepts from image descriptions, produces mostly visually identifiable concepts. The concept rating step removes non-causal concepts, enabling the full PCB-M-ReD to outperform all baselines.

#### 4.6 Analytical Studies

We perform several ablation studies and report the average accuracy across CIFAR10, CIFAR100, and CUB.

**Bottleneck Size.** We investigate how the model’s performance changes with bottleneck size. As shown in Fig. 6 (a), test accuracy improves with more concepts in the bottleneck, nearly saturating at 300. Notably, even a small bottleneck of 50 achieves reasonable accuracy. Additionally, the required bottleneck size is independent of the number of label classes.

Fewer concepts also enhance interpretability.

**Concept Creation Schemes.** We compare our concept creation scheme with: (1) LLM-generated concepts (Yang et al. 2023) and (2) “Core” WordNet concepts (Boyd-Graber et al. 2006), using the same preprocessing and selection algorithms as PCB-M-ReD. Results in Fig. 6 (a) show that our data-driven scheme outperforms both alternatives. Additionally, it avoids non-visual concepts, as confirmed by human evaluation, while also providing a performance boost.

**Concept Selection Methods.** We evaluate the effectiveness of the reconstruction-guided concept selection algorithm by comparing it with two baselines: random sampling and k-means clustering. As shown in Fig. 6 (b), our method consistently outperforms both baselines, with a noticeable performance gap at smaller bottlenecks. By selecting concepts that minimize reconstruction error, the reconstruction-guided approach ensures higher final accuracy.

**Concept Score Association.** We compare the sparsity decomposition-based concept score association and to baseline that uses CLIP similarity scores as concept scores. As shown in Fig. 6 (c), representation decomposition achieves significantly higher accuracy. By reconstructing visual representations with concepts, it ensures performance comparable to the original model, achieving higher accuracy.

**Sources of the Concepts.** Finally, we examine the impact of concept sources by using concepts extracted from different image encoders to construct CBMs. Results in Fig. 6 (d) show a performance decline when the backbones are mismatched, highlighting the importance of aligning concepts with the representational capabilities of the image encoder.

## 5 Limitations and Conclusion

In this paper, we propose PCB-M-ReD, a novel CBM that generates concepts through post-hoc decomposition of visual representations. It achieves high accuracy, zero-shot/few-shot capabilities, and built-in interpretability. However, the approach has some limitations. First, the concept generation relies on MLLMs and LLMs, which can be sub-optimal for domain-specific images that general MLLMs cannot describe precisely. Second, as a post-hoc method, the model’s performance depends on the original image encoder. We will further improve the model by designing better prompts or leveraging more advanced MLLMs.

## Acknowledgments

This research work was supported in part by the National Natural Science Foundation of China (Project No. 62322318 and No. 62201485), in part by the Research Grants Council of Hong Kong Special Administrative Region, China (Project No. T45-401/22-N).

## References

Bau, D.; Zhou, B.; Khosla, A.; Oliva, A.; and Torralba, A. 2017. Network dissection: Quantifying interpretability of deep visual representations. In *Proceedings of the IEEE conference on computer vision and pattern recognition*, 6541–6549.

Bossard, L.; Guillaumin, M.; and Van Gool, L. 2014. Food-101-mining discriminative components with random forests. In *Computer vision–ECCV 2014: 13th European conference, zurich, Switzerland, September 6–12, 2014, proceedings, part VI 13*, 446–461. Springer.

Boyd-Graber, J.; Fellbaum, C.; Osherson, D.; and Schapire, R. 2006. Adding dense, weighted connections to WordNet. In *Proceedings of the third international WordNet conference*, 29–36. Citeseer.

Bricken, T.; Templeton, A.; Batson, J.; Chen, B.; Jermyn, A.; Conerer, T.; Turner, N.; Anil, C.; Denison, C.; Askell, A.; Lasenby, R.; Wu, Y.; Kravec, S.; Schiefer, N.; Maxwell, T.; Joseph, N.; Hatfield-Dodds, Z.; Tamkin, A.; Nguyen, K.; McLean, B.; Burke, J. E.; Hume, T.; Carter, S.; Henighan, T.; and Olah, C. 2023. Towards Monosemanticity: Decomposing Language Models With Dictionary Learning. *Transformer Circuits Thread*.

Chen, C.; Li, O.; Tao, D.; Barnett, A.; Rudin, C.; and Su, J. K. 2019. This looks like that: deep learning for interpretable image recognition. *Advances in neural information processing systems*, 32.

Chen, C.; Zhang, B.; Cao, L.; Shen, J.; Gunter, T.; Jose, A. M.; Toshev, A.; Shlens, J.; Pang, R.; and Yang, Y. 2023. STAIR: learning sparse text and image representation in grounded tokens. *arXiv preprint arXiv:2301.13081*.

Cheng, G.; Han, J.; and Lu, X. 2017. Remote sensing image scene classification: Benchmark and state of the art. *Proceedings of the IEEE*, 105(10): 1865–1883.

Cherti, M.; Beaumont, R.; Wightman, R.; Wortsman, M.; Ilharco, G.; Gordon, C.; Schuhmann, C.; Schmidt, L.; and Jitsev, J. 2023. Reproducible scaling laws for contrastive language-image learning. In *Proceedings of the IEEE/CVF Conference on Computer Vision and Pattern Recognition*, 2818–2829.

Cimpoi, M.; Maji, S.; Kokkinos, I.; Mohamed, S.; and Vedaldi, A. 2014. Describing textures in the wild. In *Proceedings of the IEEE conference on computer vision and pattern recognition*, 3606–3613.

Deng, J.; Dong, W.; Socher, R.; Li, L.-J.; Li, K.; and Fei-Fei, L. 2009. Imagenet: A large-scale hierarchical image database. In *2009 IEEE conference on computer vision and pattern recognition*, 248–255. Ieee.

Fel, T.; Boutin, V.; Béthune, L.; Cadène, R.; Moayeri, M.; Andréol, L.; Chalvidal, M.; and Serre, T. 2023. A holistic approach to unifying automatic concept extraction and concept importance estimation. *Advances in Neural Information Processing Systems*, 36: 54805–54818.

Fong, R.; and Vedaldi, A. 2018. Net2vec: Quantifying and explaining how concepts are encoded by filters in deep neural networks. In *Proceedings of the IEEE conference on computer vision and pattern recognition*, 8730–8738.

Gandelsman, Y.; Efros, A. A.; and Steinhardt, J. 2023. Interpreting CLIP’s Image Representation via Text-Based Decomposition. *arXiv preprint arXiv:2310.05916*.

Gandelsman, Y.; Efros, A. A.; and Steinhardt, J. 2024. Interpreting the Second-Order Effects of Neurons in CLIP. *arXiv:2406.04341*.

Ge, Y.; Xiao, Y.; Xu, Z.; Zheng, M.; Karanam, S.; Chen, T.; Itti, L.; and Wu, Z. 2021. A peek into the reasoning of neural networks: interpreting with structural visual concepts. In *Proceedings of the IEEE/CVF Conference on Computer Vision and Pattern Recognition*, 2195–2204.

Gong, S.; Dou, Q.; and Farnia, F. 2024. Structured Gradient-based Interpretations via Norm-Regularized Adversarial Training. In *Proceedings of the IEEE/CVF Conference on Computer Vision and Pattern Recognition*, 11009–11018.

Gong, S.; Haoyu, L.; Dou, Q.; and Farnia, F. 2025a. Boosting the visual interpretability of clip via adversarial fine-tuning. In *The Thirteenth International Conference on Learning Representations*.

Gong, S.; Wang, H.; Zhang, X.; and Dou, Q. 2025b. Concepts from Neurons: Building Interpretable Medical Image Diagnostic Models by Dissecting Opaque Neural Networks. In *International Conference on Information Processing in Medical Imaging*, 3–18. Springer.

He, H.; Zhu, L.; Zhang, X.; Zeng, S.; Chen, Q.; and Lu, Y. 2025. V2C-CBM: Building Concept Bottlenecks with Vision-to-Concept Tokenizer. In *Proceedings of the AAAI Conference on Artificial Intelligence*, volume 39, 3401–3409.

Kamath, A.; Hessel, J.; and Chang, K.-W. 2023. What’s “up” with vision-language models? Investigating their struggle with spatial reasoning. In *The 2023 Conference on Empirical Methods in Natural Language Processing*.

Kim, B.; Wattenberg, M.; Gilmer, J.; Cai, C.; Wexler, J.; Viegas, F.; et al. 2018. Interpretability beyond feature attribution: Quantitative testing with concept activation vectors (tcav). In *International conference on machine learning*, 2668–2677. PMLR.

Kim, E.; Jung, D.; Park, S.; Kim, S.; and Yoon, S. 2023. Probabilistic concept bottleneck models. *arXiv preprint arXiv:2306.01574*.

Koh, P. W.; Nguyen, T.; Tang, Y. S.; Mussmann, S.; Piereson, E.; Kim, B.; and Liang, P. 2020. Concept bottleneck models. In *International conference on machine learning*, 5338–5348. PMLR.

Krizhevsky, A.; Hinton, G.; et al. 2009. Learning multiple layers of features from tiny images.

Ma, C.; Zhao, B.; Chen, C.; and Rudin, C. 2024. This looks like those: Illuminating prototypical concepts using multiple visualizations. *Advances in Neural Information Processing Systems*, 36.

Maji, S.; Rahtu, E.; Kannala, J.; Blaschko, M.; and Vedaldi, A. 2013. Fine-grained visual classification of aircraft. *arXiv preprint arXiv:1306.5151*.

Moayeri, M.; Rezaei, K.; Sanjabi, M.; and Feizi, S. 2023. Text-to-concept (and back) via cross-model alignment. In *International Conference on Machine Learning*, 25037–25060. PMLR.

Nauta, M.; Van Bree, R.; and Seifert, C. 2021. Neural prototype trees for interpretable fine-grained image recognition. In *Proceedings of the IEEE/CVF conference on computer vision and pattern recognition*, 14933–14943.

Nilsback, M.-E.; and Zisserman, A. 2008. Automated flower classification over a large number of classes. In *2008 Sixth Indian conference on computer vision, graphics & image processing*, 722–729. IEEE.

Oikarinen, T.; Das, S.; Nguyen, L. M.; and Weng, T.-W. 2023. Label-free concept bottleneck models. *arXiv preprint arXiv:2304.06129*.

Oikarinen, T.; and Weng, T.-W. 2022. Clip-dissect: Automatic description of neuron representations in deep vision networks. *arXiv preprint arXiv:2204.10965*.

Omeiza, D.; Webb, H.; Jiroka, M.; and Kunze, L. 2021. Explanations in autonomous driving: A survey. *IEEE Transactions on Intelligent Transportation Systems*, 23(8): 10142–10162.

Panousis, K. P.; Ienco, D.; and Marcos, D. 2023. Sparse linear concept discovery models. In *Proceedings of the IEEE/CVF International Conference on Computer Vision*, 2767–2771.

Pati, Y. C.; Rezaifar, R.; and Krishnaprasad, P. S. 1993. Orthogonal matching pursuit: Recursive function approximation with applications to wavelet decomposition. In *Proceedings of 27th Asilomar conference on signals, systems and computers*, 40–44. IEEE.

Pratt, S.; Covert, I.; Liu, R.; and Farhadi, A. 2023. What does a platypus look like? generating customized prompts for zero-shot image classification. In *Proceedings of the IEEE/CVF International Conference on Computer Vision*, 15691–15701.

Radford, A.; Kim, J. W.; Hallacy, C.; Ramesh, A.; Goh, G.; Agarwal, S.; Sastry, G.; Askell, A.; Mishkin, P.; Clark, J.; et al. 2021. Learning transferable visual models from natural language supervision. In *International conference on machine learning*, 8748–8763. PMLR.

Rao, S.; Mahajan, S.; Böhle, M.; and Schiele, B. 2024. Discover-then-Name: Task-Agnostic Concept Bottlenecks via Automated Concept Discovery. In *European Conference on Computer Vision*.

Rudin, C. 2019. Stop explaining black box machine learning models for high stakes decisions and use interpretable models instead. *Nature machine intelligence*, 1(5): 206–215.

Saha, O.; Van Horn, G.; and Maji, S. 2024. Improved Zero-Shot Classification by Adapting VLMs with Text Descriptions. In *Proceedings of the IEEE/CVF Conference on Computer Vision and Pattern Recognition*, 17542–17552.

Selvaraju, R. R.; Cogswell, M.; Das, A.; Vedantam, R.; Parikh, D.; and Batra, D. 2017. Grad-cam: Visual explanations from deep networks via gradient-based localization. In *Proceedings of the IEEE international conference on computer vision*, 618–626.

Shang, C.; Zhou, S.; Zhang, H.; Ni, X.; Yang, Y.; and Wang, Y. 2024. Incremental residual concept bottleneck models. In *Proceedings of the IEEE/CVF Conference on Computer Vision and Pattern Recognition*, 11030–11040.

Simonyan, K.; Vedaldi, A.; and Zisserman, A. 2013. Deep inside convolutional networks: Visualising image classification models and saliency maps. *arXiv preprint arXiv:1312.6034*.

Soomro, K. 2012. UCF101: A dataset of 101 human actions classes from videos in the wild. *arXiv preprint arXiv:1212.0402*.

Srivastava, D.; Yan, G.; and Weng, L. 2024. Vlg-cbm: Training concept bottleneck models with vision-language guidance. *Advances in Neural Information Processing Systems*, 37: 79057–79094.

Tan, A.; Zhou, F.; and Chen, H. 2024a. Explain via Any Concept: Concept Bottleneck Model with Open Vocabulary Concepts. *arXiv preprint arXiv:2408.02265*.

Tan, A.; Zhou, F.; and Chen, H. 2024b. Post-hoc Part-prototype Networks. *arXiv preprint arXiv:2406.03421*.

Tschandl, P.; Rosendahl, C.; and Kittler, H. 2018. The HAM10000 dataset, a large collection of multi-source dermatoscopic images of common pigmented skin lesions. *Scientific data*, 5(1): 1–9.

Vielhaben, J.; Bluecher, S.; and Strodthoff, N. 2023. Multi-dimensional concept discovery (MCD): A unifying framework with completeness guarantees. *arXiv preprint arXiv:2301.11911*.

Wah, C.; Branson, S.; Welinder, P.; Perona, P.; and Belongie, S. 2011. The caltech-ucsd birds-200-2011 dataset.

Yang, Y.; Panagopoulou, A.; Zhou, S.; Jin, D.; Callison-Burch, C.; and Yatskar, M. 2023. Language in a bottle: Language model guided concept bottlenecks for interpretable image classification. In *Proceedings of the IEEE/CVF Conference on Computer Vision and Pattern Recognition*, 19187–19197.

Yuksekgonul, M.; Wang, M.; and Zou, J. 2022. Post-hoc concept bottleneck models. *arXiv preprint arXiv:2205.15480*.

Yun, T.; Bhalla, U.; Pavlick, E.; and Sun, C. 2022. Do Vision-Language Pretrained Models Learn Composable Primitive Concepts? *arXiv preprint arXiv:2203.17271*.

Zarlenga, M. E.; Barbiero, P.; Ciravagna, G.; Marra, G.; Giannini, F.; Diligenti, M.; Shams, Z.; Precioso, F.; Melacci, S.; Weller, A.; et al. 2022. Concept embedding models: Beyond the accuracy-explainability trade-off. *arXiv preprint arXiv:2209.09056*.

## A Dataset Statistics

Table 3 depicts detailed statistics for all datasets. We follow the same train/dev/test splits provided by LaBo (Yang et al. 2023). For ImageNet, we only evaluate the dev set.

## B Implementation Details

### B.1 Linear Probe

The test accuracy of the CLIP linear probe is referenced from (Yang et al. 2023), which utilizes encoded images prior to their projection into the vision-text embedding space as inputs for the classifier. In our approach, we employ the approximated visual embedding—already situated in the vision-text embedding space—as the classifier’s input. We implement logistic regression using sklearn’s L-BFGS, allowing for a maximum of 1,000 iterations. To find the optimal values for the hyperparameter  $C$ , we perform a binary search on the validation set, starting with the range  $[1e^6, 1e^4, 1e^2, 1, 1e^{-2}, 1e^{-4}, 1e^{-6}]$ . After establishing the left and right bounds for  $C$ , we iteratively halve the interval over 8 steps to arrive at the final hyperparameter value.

### B.2 Training of Sparse Autoencoder

We train sparse autoencoders following the setup of (Bricken et al. 2023). Specifically, we utilize the implementation from sparse autoencoder library. For each dataset, we train on the training data for 200 epochs, with expansion factor of 4. We perform hyperparameter sweeps based on the  $L_2$  reconstruction errors of the validation set over the learning rate with the range  $[1e^{-5}, 5e^{-5}, 1e^{-4}, 5e^{-4}, 1e^{-3}]$  and  $L_1$  sparsity coefficient with the range  $[3e^{-5}, 1.5e^{-4}, 3e^{-4}, 1.5e^{-3}, 3e^{-3}]$ .

### B.3 Sparse Decomposition

We utilize scikit-learn’s implementation of orthogonal matching pursuit for sparse decomposition. The orthogonal matching pursuit has a parameter, i.e., number of non-zero coefficients, which controls the sparsity of the decomposition. For the visual representation of each sample, we use binary search within the range  $[650, \text{full}]$  to tune this parameter, based on the  $L_2$  reconstruction error of the visual representation. Here “full” refers to the total number of concepts within the candidate pool. The specific hyper-parameters can be found in the released code.

### B.4 Prompts

**Object Description.** We ask the MLLMs to describe the objects with the following prompts. Specifically, we apply a two phase prompt. We first use the prompt-1, which ask the MLLMs to use chain-of-thought to determine the category of the object within the image. Then we use the prompt-2 to ask the MLLMs to summarize the reasoning process of the first stage, and give a concise description of the subject.

- **Food-101:**

- prompt-1 *What is the food? Use chain of thought to reason and list all the visual features that lead to the conclusion.*

Name	n. of classes	n. of images		
		Train	Dev	Test
Food-101	101	50,500	20,200	30,300
FGVC-Aircraft	102	3,334	3,333	3,333
Flower-102	102	4,093	1,633	2,463
CUB-200-2011	200	3,994	2,000	5,794
UCF-101	101	7,639	1,898	3,783
DTD	47	2,820	1,128	1,692
HAM10000	7	8,010	1,000	1,005
RESISC45	45	3,150	3,150	25,200
CIFAR-10	10	45,000	5,000	10,000
CIFAR-100	100	45,000	5,000	10,000
ImageNet	1,000	1,281,167	50,000	-

Table 3: Detailed statistics of the 11 datasets.

- prompt-2 *Briefly summarize the appearance of the food in one paragraph. Do not mention what the food is.*
- **FGVC-Aircraft:**
  - prompt-1 *What is the model of the flight? Use chain of thought to reason and list all the visual features that lead to the conclusion.*
  - prompt-2 *Concisely summarize the appearance of the flight using one paragraph. Do not include the specific model name.*
- **Flower-102:**
  - prompt-1 *What is the species of the flower? Use chain of thought to reason and list all the visual features that lead to the conclusion.*
  - prompt-2 *Concisely summarize the appearance of the flower using one paragraph. Do not include the specific species name of the flower.*
- **CUB-200-2011:**
  - prompt-1 *What is the species of the bird? Use chain of thought to reason and list all the visual features that lead to the conclusion.*
  - prompt-2 *Concisely summarize the appearance of the bird using one paragraph. Do not include the specific species name of the bird.*
- **UCF-101:**
  - prompt-1 *What is the action the characters are performing? Use chain of thought to reason and list all the visual features that lead to the conclusion.*
  - prompt-2 *Briefly summarize visual pattern of the action using one paragraph. Do not mention what the action is.*
- **DTD:**
  - prompt-1 *What is the texture (e.g., blotchy, frilly)? Use chain of thought to reason and list all the visual features that lead to the conclusion.*
  - prompt-2 *Briefly summarize the feature of the texture in one paragraph, do not mention the name of the texture.*

- **HAM10000:**
  - prompt-1 *What is the type of the pigmented lesion in the dermatoscopic image (e.g., Actinic keratoses, basal cell carcinoma, benign keratosis-like lesions, dermatofibroma, melanoma, melanocytic nevi, and vascular lesions)? Use chain of thought to reason and list all the visual features that lead to the conclusion.*
  - prompt-2 *Briefly summarize the appearance of the pigmented lesion in one paragraph, do not include the specific type name.*
- **RESISC45:**
  - prompt-1 *What is the scene class in the satellite image? Use chain of thought to reason and list all the visual features that lead to the conclusion.*
  - prompt-2 *Briefly summarize the appearance of the scene in one paragraph. Do not mention what the scene is.*
- **CIFAR-10:**
  - prompt-1 *Describe the appearance of the object within the image. Only include the visual features that can help identify its category. Use Chain-of-thought to reason.*
  - prompt-2 *Briefly summarize the appearance of the object in one paragraph. Do not mention what the object is.*
- **CIFAR-100:**
  - prompt-1 *Describe the appearance of the object within the image. Only include the visual features that can help identify its category. Use Chain-of-thought to reason.*
  - prompt-2 *Briefly summarize the appearance of the object in one paragraph. Do not mention what the object is.*
- **ImageNet:**
  - prompt-1 *Describe the appearance of the object within the image. Only include the visual features that can help identify its category. Use Chain-of-thought to reason.*
  - prompt-2 *Briefly summarize the appearance of the object in one paragraph. Do not mention what the object is.*

**Concept Summarization.** Once we have descriptions for each image, we gather the descriptions for the top 20 activations in each potential concept. We then utilize the prompt shown in Fig. 7 to request LLMs to summarize these descriptions and suggest candidate concepts. The tasks description is tailored according to the specific dataset (e.g., for CUB-200-2011, the task description is “bird species classification”). Finally, we follow (Yang et al. 2023) to replace the specific name of the category by its higher level class name (e.g., specific bird species name is replaced with “bird”).

**Concept Rating.** Once we obtain a pool of candidate concepts, we ask LLMs to rate each concepts according to their

relevancy to the specific tasks. The prompt we use is presented in Fig. 8. Each candidate is given a score between 1 to 10 according to its quality. We only keep concepts with score greater than 6 for the subsequent processing.

## B.5 Human Evaluation

Here we describe the details how we design the user study to evaluate the interpretability of the proposed PCB-M-ReD and the baselines.

**Method.** To perform human evaluation, we randomly sample several images from the test set of ImageNet (Deng et al. 2009), Food-101 (Bossard, Guillaumin, and Van Gool 2014), UCF-101 (Soomro 2012), CUB-200-2011 (Wah et al. 2011), and Flower-102 (Nilsback and Zisserman 2008). The samples selected all have correct prediction by the corresponding methods. We select these five datasets because they are common objects that can be evaluated with common knowledge. For each image, we use either PCB-M-ReD, PCB-M-ReD without the LLMs-based concept scoring, or LaBo (Yang et al. 2023) to generate explanations. We generate explanations for multiple images, i.e., different users will see different cases.

**Question Structure.** For each question, we show the volunteer three statement, and ask them to select whether they agree with the statement. The statement includes: 1) The explanations are visually identifiable features, 2) The explanations faithfully describe the image, 3) There is a clear causal relationship between the explanation and the prediction. We ask the volunteers to rate on a scale of 1 and 5, with 1 to be very disagree with the statement and 5 to be very agree with the statement.

**Survey Structure.** For each volunteers, we randomly sample 2 methods out of 3 methods, and show the images and the corresponding explanations sampled from 5 datasets. The order of the images are also shuffled. Each volunteer will see 10 images and answer 30 questions in total. Fig. 11 shows a sample survey. We published the survey internally, and received 39 responses.

**Ethic Statement** In our user study, we did not collect any user information. The IRB review is waived because the study does not involve human subjects as defined in 45 CFR 46.102(f).

## C Derivation of Alg. 1

In this section, we provide more explanation on the Alg. 1. We start with the optimization objective:

$$\min_{\mathcal{C}} \sum_{i=1}^N \min_{\beta_i(\mathcal{C})} \|\mathbf{I}_i - \mathbf{R}(\mathcal{C})^T \beta_i(\mathcal{C})\|_F^2. \quad (3)$$

We notice the inner minimization problem has analytical solution:

$$\beta_i^*(\mathcal{C}) = (\mathbf{R}(\mathcal{C})\mathbf{R}(\mathcal{C})^T)^{-1} \mathbf{R}(\mathcal{C})\mathbf{I}_i. \quad (4)$$

The greedy algorithm works by incrementally adding new concept into  $\mathcal{C}$ . Assume we already have  $n$  element in  $\mathcal{C}_n$ .

You are a data scientist . We 're studying neurons in an image neural network , where each neuron detects specific concepts in images . The neural network is trained to conduct [tasks description](#) . I 've identified the images that most strongly activate a particular neuron and will provide you with their associated text descriptions of the image . Your task is to analyze these descriptions and determine the common concept that this neuron is detecting .

To arrive at the most accurate and precise explanation of what this neuron is detecting , you must engage in explicit chain of thought reasoning . Begin by thoroughly examining all provided image captions , noting any patterns or commonalities . Pay close attention to recurring terminology , described structures , and consistent visual features . Consider how these elements might interrelate to form a singular , distinctive concept that the neuron could be identifying . Evaluate the context of image and consider which aspects would be most significant or unique within this classification task .

As you progress through your analysis , verbalize your thought process . Explain each step of your reasoning , from initial observations to intermediate conclusions , and finally to your overall assessment . This chain of thought approach will help ensure a comprehensive and well - reasoned final explanation .

After this detailed analytical process , formulate a single , specific explanation of what the neuron is detecting . Your explanation should be as precise and fine - grained as possible , avoiding vague or general statements . Focus on specific concept or combinations of concepts . Refrain from explaining the bird species itself ( e . g ., avoid statements like " This feature represents X, which is characterized by ..." ) . Base your explanation solely on the information provided in the reports , without additional domain knowledge that might not be captured by the neuron .

Come up with 10 distinct concepts that are more likely to be associated with the neuron . Please write a list of captions ( separated by bullet points " \* " ) . For example :

- \* "a dog next to a horse"
- \* "a car in the rain"
- \* "low quality"
- \* "cars from a side view"
- \* "people in a intricate dress"
- \* "a joyful atmosphere"

The hypothesis should be a caption, so hypotheses like "more of ...", "presence of ...", "images with ..." are incorrect. Also do not enumerate possibilities within parentheses. Here are examples of bad outputs and their corrections:

- \* INCORRECT: "various nature environments like lakes, forests, and mountains" CORRECTED: "nature"
- \* INCORRECT: "images of household object (e.g. bowl, vacuum, lamp)" CORRECTED: "household objects"
- \* INCORRECT: "Presence of baby animals" CORRECTED: "baby animals"
- \* INCORRECT: "Different types of vehicles including cars, trucks, boats, and RVs" CORRECTED: "vehicles"
- \* INCORRECT: "Images involving interaction between humans and animals" CORRECTED: "interaction between humans and animals"
- \* INCORRECT: "More realistic images" CORRECTED: "realistic images"
- \* INCORRECT: "Insects (cockroach, dragonfly, grasshopper)" CORRECTED: "insects"

Below are the image descriptions , listed in order of how strongly they activate the neuron . Use these to inform your analysis and final explanation :

<Description 1>  
<Description 2>  
<...>

Figure 7: Prompt used for summarizing the descriptions and generating candidate concepts.

At the  $n + 1$  step, we will find the optimal concept  $c^*$  that minimize the objective:

$$\min_c \sum_{i=1}^N \|\mathbf{I}_i - \mathbf{R}(\mathcal{C}_n \cup \{c\})^T (\mathbf{R}(\mathcal{C}_n \cup \{c\})\mathbf{R}(\mathcal{C}_n \cup \{c\})^T)^{-1} \mathbf{R}(\mathcal{C}_n \cup \{c\})\mathbf{I}_i\|_F^2. \quad (5)$$

A vanilla way to calculate  $c^*$  is to enumerate all  $c \in \mathcal{C}_0$  and compute the objective value, and select the  $c^*$  that minimize the objectives. However, this can be computational expensive especially when the size of  $\mathcal{C}_0$  is very large. However, we notice that

$$\mathbf{R}(\mathcal{C}_n \cup \{c\})^T (\mathbf{R}(\mathcal{C}_n \cup \{c\})\mathbf{R}(\mathcal{C}_n \cup \{c\})^T)^{-1} \mathbf{R}(\mathcal{C}_n \cup \{c\}) \\ = [\mathbf{R}(\mathcal{C}_n)^T, \mathcal{T}(c)] \begin{bmatrix} \mathbf{R}(\mathcal{C}_n)\mathbf{R}(\mathcal{C}_n)^T & \mathbf{R}(\mathcal{C}_n)\mathcal{T}(c) \\ \mathcal{T}(c)^T\mathbf{R}(\mathcal{C}_n)^T & \mathcal{T}(c)^T\mathcal{T}(c) \end{bmatrix}^{-1} \begin{bmatrix} \mathbf{R}(\mathcal{C}_n) \\ \mathcal{T}(c)^T \end{bmatrix}$$

By defining  $\mathbf{A} = (\mathbf{R}(\mathcal{C}_n)^T\mathbf{R}(\mathcal{C}_n))^{-1}$ ,  $\mathbf{P} = \mathbf{R}(\mathcal{C}_n)(\mathbf{R}(\mathcal{C}_n)^T\mathbf{R}(\mathcal{C}_n))^{-1}\mathbf{R}(\mathcal{C}_n)^T$  and  $z = \mathcal{T}(c)^T\mathcal{T}(c) -$

$\mathcal{T}(c)^T P \mathcal{T}(c)$ , we have:

$$\begin{bmatrix} \mathbf{R}(\mathcal{C}_n)\mathbf{R}(\mathcal{C}_n)^T & \mathbf{R}(\mathcal{C}_n)\mathcal{T}(c) \\ \mathcal{T}(c)^T\mathbf{R}(\mathcal{C}_n)^T & \mathcal{T}(c)^T\mathcal{T}(c) \end{bmatrix}^{-1} \\ = \begin{bmatrix} \mathbf{A} + \mathbf{A}\mathbf{R}(\mathcal{C}_n)\mathcal{T}(c)\mathcal{T}(c)^T\mathbf{R}(\mathcal{C}_n)^T\mathbf{A}/z & -\mathbf{A}\mathbf{R}(\mathcal{C}_n)\mathcal{T}(c)/z \\ -\mathcal{T}(c)^T\mathbf{R}(\mathcal{C}_n)^T\mathbf{A}/z & 1/z \end{bmatrix}.$$

Therefore, we find that we do not need to recalculate the matrix inverse for every  $c \in \mathcal{C}_0$ , which is the most time-consuming operation. Instead, we only need to calculate  $\mathbf{A} = (\mathbf{R}(\mathcal{C}_n)^T\mathbf{R}(\mathcal{C}_n))^{-1}$  once, and the result can be reused for all  $c$ . By further simplifying the formula, we have

$$\mathbf{R}(\mathcal{C}_n \cup \{c\})^T (\mathbf{R}(\mathcal{C}_n \cup \{c\})\mathbf{R}(\mathcal{C}_n \cup \{c\})^T)^{-1} \mathbf{R}(\mathcal{C}_n \cup \{c\}) \\ = \mathbf{P}\mathbf{Q}\mathbf{P} - \mathbf{Q}\mathbf{P} - \mathbf{P}\mathbf{Q} + \mathbf{P} + \mathbf{Q},$$

where  $\mathbf{Q} = \mathcal{T}(c)\mathcal{T}(c)^T/z$ . This gives the exact algorithm as Alg. 1. For each  $c$ , we reuse the common  $\mathbf{P}$  and recalculate  $\mathbf{Q}$ . The calculation of  $\mathbf{Q}$  only entails matrix multiplication and scalar division, being more efficient than the original formula which entails matrix inversion. Note that the simplification holds if and only if  $z \neq 0$ . The condition  $z = 0$

I want to extract some concepts for `<task description>`. Here are the candidates:

```
<concept 1>
<concept 2>
<...>
```

I want you to score these concepts according to their relevancy to the task of `<task description>`. A good concept should describe detailed characteristics of the `<classification target>`, and be discriminative among different classes. The feature should also be subjective and visually identifiable. Also try to avoid use shortcut features such as unrelated background and objective evaluation.

Each concept receives an overall score on a scale of 1 to 10, where a higher score indicates better overall performance.

Please first output a single line containing only ten values indicating the scores for each concept, respectively. The scores are separated by a space.

In the subsequent line, please provide a comprehensive explanation of your evaluation, avoiding any potential bias and ensuring that the order in which the responses were presented does not affect your judgment.

Figure 8: Prompt used for rating the candidate concepts.

means there is linear dependency between  $c$  and existing elements within  $\mathcal{C}_n$ . To guarantee the selected concepts are independent, we should remove such  $c$ .

## D Additional Results

### D.1 Full Few-shot Performance Result

We present the full few-shot performance result in Fig. 9. We show the test accuracy of 1, 2, 4, 8, and 16-shot on 11 datasets. The shot refers to the labeled image per classes during training phase. Since the concept extraction and selection stages are conducted in an unsupervised manner, we still utilize all the training data for concept extraction and selection (i.e., the concepts used for building CBMs are the same as that for fully-supervised setting). The results demonstrate that PCB-M-ReD consistently outperforms baselines across different tasks and settings.

### D.2 Complete Results of Human Evaluation

In Fig. 10, we present the complete human evaluation results. We observe that, for most datasets, PCB-M-ReD significantly outperforms LaBo. However, there are still instances of failure. For example, in the case of the food dataset, PCB-M-ReD achieved lower scores than LaBo. This is likely because MLLMs struggle to describe the visual patterns of food without explicitly naming it, especially when the ingredients have been processed and is hard to distinguish. In contrast, LLMs tend to describe food based on its ingredients and cooking methods, resulting in more accurate concepts.

### D.3 Additional Qualitative Result

In this section, we present additional qualitative examples for the remaining six datasets in Fig. 12. Our method offers coherent explanations for its predictions.

### D.4 Statistical Significance

To verify the improvements of PCB-M-ReD over baselines, we perform statistical test. We perform Wilcoxon signed-rank (WSR) tests on the accuracy over 11 datasets, yielding p-values of 0.005 (vs. LaBo), 0.001 (vs. Res-CBM),

and 0.002 (vs. V2C-CBM), showing statistically significant improvements over baselines. For the results of user study shown in Fig. 5, we also perform WSR test and the result shows  $p < 0.05$  for all pairs.

### D.5 Extension to non-CLIP Model

The PCB-M-ReD framework can be extended to non-CLIP models with simple modifications, as its core components: concept extraction, concept selection, and representation decomposition, are not tied to CLIP. For non-CLIP models, techniques like concept activation vectors (CAVs) (Kim et al. 2018) can be used to construct concept representations, bypassing the need for a text encoder. Given a candidate concept and captions for several images, we can prompt the LLM to determine whether each image contains the concept. This results in multiples positive and negative samples. These samples are then used to derive CAVs as the concept representation. Gong et al. (2025b) gives details of non-CLIP extesion of PCB-M-ReD.

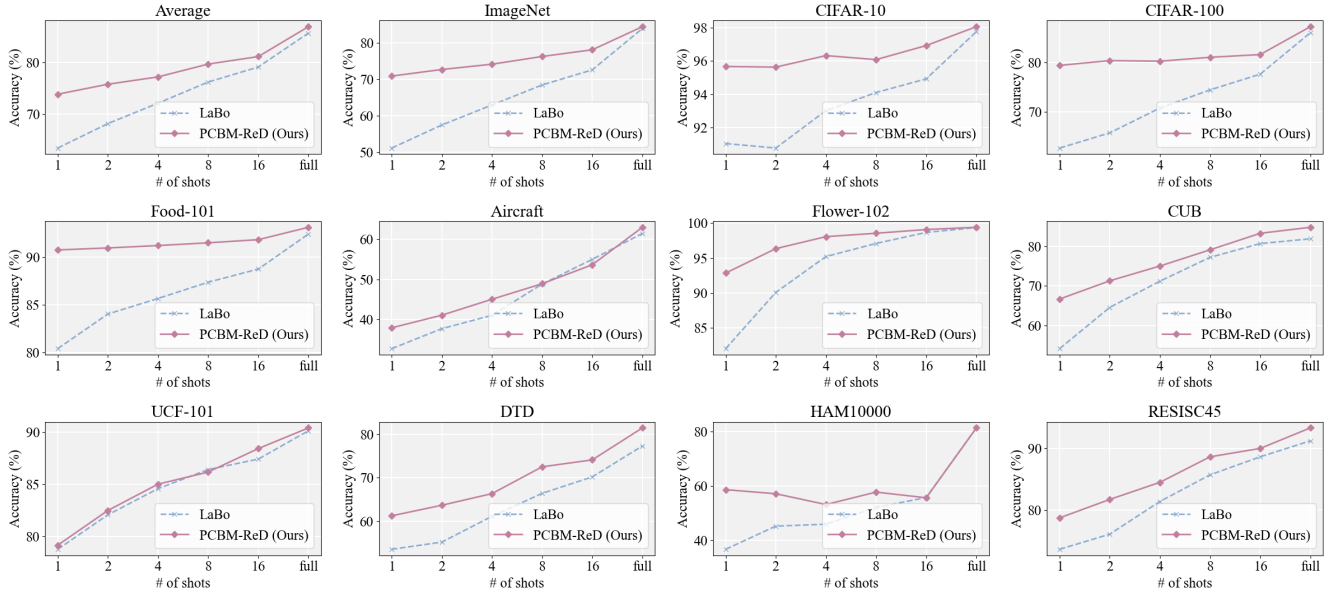


Figure 9: Few-shot test accuracy (%) comparison between PCBM-ReD and LaBo on 11 datasets. The x-axis represents the number of labeled images for each class.

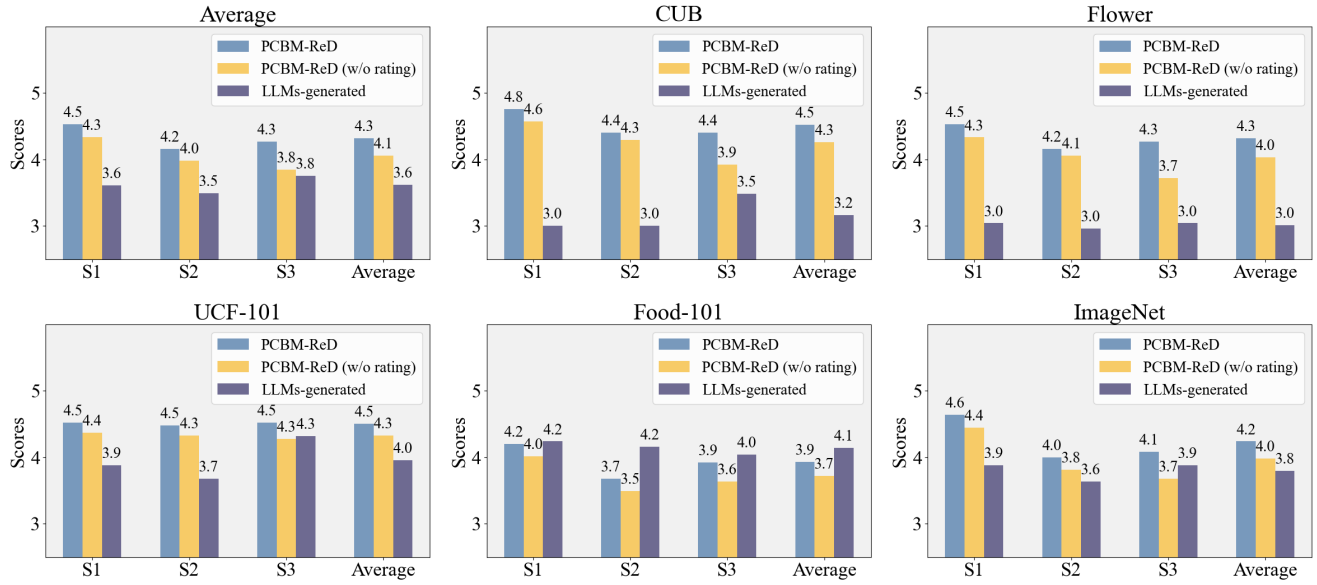


Figure 10: Full results of user studies. We show the average scores for 5 individual datasets.

Below are the inputs and predictions of an image classification model. We present explanations for why the model makes specific predictions. Please help evaluate the quality of these explanations.



**Prediction** lorikeet

**Explanations**

1. brightly colored plumage with green, blue, and red feathers
2. stunning bird that is full of color
3. beautiful bird with a bright, colorful beak

Q1. The explanations are visually identifiable features.

disagree  1  2  3  4  5 agree

Q2. The explanations faithfully describe the image

disagree  1  2  3  4  5 agree

Q3. There is a clear causal relationship between the explanation and the prediction.

disagree  1  2  3  4  5 agree



**Prediction** foxglove

**Explanations**

1. is also known as the hollyhock
2. used in medicinal teas and tinctures
3. beautiful deep pink color

Q1. The explanations are visually identifiable features.

disagree  1  2  3  4  5 agree

Q2. The explanations faithfully describe the image

disagree  1  2  3  4  5 agree

Q3. There is a clear causal relationship between the explanation and the prediction.

disagree  1  2  3  4  5 agree

Figure 11: Examples of questions in the user study. For each volunteer, we show the image, the prediction, and the corresponding explanations. We ask the user to select whether they agree with certain statements.

	Class Name	Top Concepts	Class Name	Top Concepts	Class Name	Top Concepts	Class Name	Top Concepts
DTD	<b>braided</b> 	1. tightly woven, repeating pattern 2. Metallic surface with holes 3. woven texture with grid-like patterns of loops	<b>chequered</b> 	1. a fabric with a repeating pattern of black and white squares 2. high-contrast black and white patterns	<b>fibrous</b> 	1. surface with raised patterns 2. fabric with interlocking threads 3. Woven texture with tightly packed fibers	<b>perforated</b> 	1. rough industrial grating 2. three-dimensional textured surface 3. rough texture with raised dots
aircraft	<b>DHC-8-100</b> 	1. a turboprop plane with a red, white and blue livery 2. a turboprop aircraft with a T-tail and a specific color scheme	<b>E-195</b> 	1. jet airliner with a winglet at the wingtip 2. narrow-body jet with a curved nose 3. under-wing engines	<b>Model B200</b> 	1. a turboprop airliner with two large propellers 2. a turboprop plane with blue and white color scheme and window placement	<b>Saab 2000</b> 	1. a turboprop aircraft with a T-tail and a specific color scheme 2. Turboprop aircraft with propellers
RESISC45	<b>railway station</b> 	1. a train yard with multiple tracks and sidings 2. transportation hub with open areas 3. railroad yard with multiple tracks	<b>baseball diamond</b> 	1. a baseball field surrounded by fences and dugouts 2. a baseball field with basepaths 3. grid-like urban area	<b>beach</b> 	1. rocky shoreline surrounded by expanse of water 2. large lake with sandy shoreline 3. peninsula extends into water	<b>chaparral</b> 	1. vast, arid landscape with small dunes 2. rugged mountainous area with sparse vegetation
Food101	<b>beef tartare</b> 	1. cylindrical food item topped with red and yellow condiments 2. a crispy and caramelized meat centerpiece	<b>bibimbap</b> 	1. a bowl of white rice with colorful vegetables and a fried egg 2. a colorful display of raw fish, rice, and vegetables	<b>cheesecake</b> 	1. a mousse-like cake with a cream filling 2. sweet treat with fruit and chocolate toppings	<b>baklava</b> 	1. a round, flaky pastry with visible filling 2. a golden-brown pastry with a spiral pattern
UCF101	<b>band marching</b> 	1. a synchronized marching formation on a street 2. a group wearing matching uniforms 3. orchestral performances	<b>military parade</b> 	1. a synchronized marching formation on a street 2. banners and flags 3. a group in uniforms marching in unison	<b>biking</b> 	1. a person riding a bicycle on a paved path 2. characters pedaling bicycles 3. dynamic poses of cyclists in motion	<b>cliff diving</b> 	1. a dynamic athletic pose 2. splash from a high jump to a pool 3. pose with bodies arched and limbs outstretched
CIFAR-10	<b>automobile</b> 	1. a red vehicle with a curved front end 2. a car with a curved roofline 3. a vibrant-colored car with contrasting features	<b>bird</b> 	1. an animal with white plumage and a long, curved beak 2. animal perched on a wooden post 3. close-up of a animal's head	<b>airplane</b> 	1. a modern aircraft with swept-back wings 2. pointed aircraft with angled wings 3. white commercial airliner	<b>deer</b> 	1. majestic animal with curved antlers 2. blurry animal with antlers 3. four-legged animal with antlers
CIFAR-100	<b>apple</b> 	1. red fruit with a stem 2. round, orange-colored fruits 3. fruit with a hard pit	<b>beaver</b> 	1. a multi-legged creature 2. a dark gray creature 3. quadruped with light brown fur and darker patches	<b>bowl</b> 	1. smooth, round container with a warm earthy color 2. branded food or beverage container 3. multicolored sphere	<b>lawn mower</b> 	1. vibrant green tool with a curved handle 2. walk-behind lawn care tool 3. a functional object with blades

Figure 12: Several example explanations generated by PCB-M-ReD. The examples are sampled from the test set of 7 datasets uncovered by the main paper, which have correct predictions. We also show their corresponding top concepts that contribute the most to the logits.